Credibility analysis of computational fluid dynamic simulations for compound channel flow

M. S. Filonovich, R. Azevedo, L. R. Rojas-Solórzano and J. B. Leal

ABSTRACT

In this paper, verification and validation of a turbulence closure model is performed for an experimental compound channel flow, where the velocity and turbulent fields were measured by a Laser Doppler Velocimeter (LDV). Detailed Explicit Algebraic Reynolds Stress Model (EARSM) simulations are reported. There are numerous methods and techniques available to evaluate the numerical uncertainty associated with grid resolution. The authors have adopted the Grid Convergence Index (GCI) approach. The velocity components, the turbulence kinetic energy (TKE), the dissipation rate and the Reynolds stresses were used as variables of interest. The GCI results present low values for the u velocity component, but higher values in what concerns the v velocity component and w velocity component (representing secondary flows) and for Reynolds stresses $RSxy$ and $RSyz$. This indicates that the mean flow has converged but the turbulent field and secondary flows still depend on grid resolution. Based on GCI values distribution, the medium and fine meshes were further refined. In addition to GCI analysis, the authors have performed linear regression analysis for estimating the mesh quality in what concerns small value variables. Comparison of numerical and experimental results shows good agreement.

Key words | compound channel flow, Grid Convergence Index (GCI), Reynolds stresses, validation and verification, velocity components

M. S. Filonovich (corresponding author)
R. Azevedo
J. B. Leal
Department of Civil Engineering,
Faculdade de Ciências e Tecnologia da
    Universidade Nova de Lisboa,
Campus de Caparica,
2829-516, Caparica,
Portugal
E-mail: *m.filonovich@fct.unl.pt*

M. S. Filonovich
J. B. Leal
CEHIDRO,
Instituto Superior Técnico,
Av. Rovisco Pais,
1049-001, Lisbon,
Portugal

L. R. Rojas-Solórzano
Department of Energy Conversion and Transport,
Universidad Simón Bolívar,
AP 1080, Caracas,
Venezuela

NOTATION

h_1, h_2, h_3	grid size of fine-, medium- and coarse-grid, respectively, m;	i	subscript that stands for local values in the ith cell;
ΔV_i	volume of ith cell, m^3;	p	apparent order of accuracy;
N	total number of cells of the calculation domain;	H	water level above channel bottom, m;
r_{21}, r_{32}	refinement factor between fine mesh 1 and medium mesh 2, and between medium mesh 2 and coarse mesh 3, respectively;	h_b	bankfull level above channel bottom, m;
		S_0	bed slope of the flume;
		B	section width, m;
e_a^{21}, e_a^{32}	approximate relative error between meshes 1 and 2, and between meshes 2 and 3, respectively;	b	main channel bottom width, m;
		z^+	non-dimensional vertical coordinate;
		h_r	relative flow depth;
f_1, f_2, f_3	fine-, medium- and coarse-grid solution of a variable of interest obtained with grid spacing h_1, h_2 and h_3, respectively;	u, v, w	longitudinal, transversal and vertical velocity components, respectively, m/s;
		TKE	turbulence kinetic energy per unit mass, m^2/s^2;
F_s	safety factor;	dissipation	dissipation rate per unit mass, m^2/s^3;

RSxy, RSxz, RSyz	tangential Reynolds stresses, N/m^2;
GCI21, GCI32	Grid Convergence Index values between meshes 1 and 2, and between meshes 2 and 3, respectively;
GCI21r, GCI32r	Grid Convergence Index values between refined meshes 1 and 2, and between mesh 2 refined and mesh 3, respectively;
R	correlation coefficient;
–	overbar operator that stands for global (cross-section averaged) values.

INTRODUCTION

During recent decades, there has been an incredible increase in computer simulations of practical fluid dynamics problems. There are currently many commercial and in-house computational fluid dynamics (CFD) codes that simulate the behaviour of turbulent flows. A CFD code is expected to be a very powerful tool, as far as it can help solving very important but difficult to measure flows. Furthermore, nowadays in many applications of CFD it is no longer enough just to produce a solution; the credibility analysis of the numerical model should be performed. This analysis consists of two fundamental steps: verification and validation (V&V).

Verification is principally a mathematical and computer science issue (Roache 1998a), which consists of two steps:

1. Code verification, its assessment consists of accumulating evidence certifying that the code does not have algorithmic or programming errors.
2. Solution verification is based on the accumulation of evidence that a specific calculation is correct and accurate, and requires confirmation of grid convergence (Oberkampf & Trucano 2002).

Validation is primarily a physical sciences issue (Roache 1998a), which shows the assessment of the accuracy of a computational model by comparison with experimental data, direct numerical simulation (DNS) or analytical solution, when available. In other words, according to

Roache (1994) verification is 'solving the equations right' and validation is 'solving the right equations'.

CFD was one of the first fields to seriously begin developing concepts and procedures for V&V methodology. There are a number of authors who have contributed to the verification of CFD solutions, like Celik *et al.* (1993), Roache (1997, 1998a, b) and many others. Some of these authors have contributed highly accurate numerical solutions, while others have contributed analytical solutions useful for verification. A large number of researches through the years have conducted the work in validation methodology and validation experiments (e.g., Celik *et al.* 1994; Oberkampf 1994; Coleman & Stern 1997; Roache 1998a).

The first quality-control measures in the CFD area were issued by the editors of the American Society of Mechanical Engineers (ASME) *Journal of Fluids Engineering* (JFE) in 1986 by publishing a brief policy statement (Roache *et al.* 1986) which was expanded in 1993 (Freitas 1993). Since then, for further improvement of quality of publications in the CFD community, the discretization error estimation is required to publish numerical results in many CFD journals. There are recommended procedures and guidelines to be followed in order to make sure that a numerical solution has reached a certain level of accuracy. In this paper, authors follow the *Journal of Fluids Engineering* editorial policy statement on the control of numerical accuracy. These statements emphasize that for a CFD simulation to be credible, the code needs to be verified and validated (comparison with reliable experimental results, DNS or analytical solution if available).

Code verification will not be addressed; it is assumed that the commercial code ANSYS CFX 12.0, used in this paper, itself has been verified independently by many authors that have been using this code for numerical simulations and have published their results. ANSYS CFX has been used to consider flow structures in experimental channels such as the Flood Channel Facility (Morvan *et al.* 2002; Morvan 2005).

Furthermore, work on CFD based on large eddy simulation (LES) has been performed by Sterling *et al.* (2008) to detail the physics of rectangular channel flows.

Despite all these applications, there has been almost no attention given in compound channel flow studies to the

issue of solution credibility. The work carried out here aims to evaluate the level of accuracy of CFD calculations compared with experimental data. For compound channel flow solution verification, where the correct solution is unknown, the authors have adopted a Grid Convergence Index (GCI). In the case of small value variables, the GCI approach results in 'unrealistic' high GCI values, and therefore the approach was complemented with a linear regression analysis that seems more appropriated to deal with low magnitude variables, like v and w velocity components and Reynolds stresses.

For validation of the solution, comparison of numerical results obtained by turbulence closure Explicit Algebraic Reynolds Stress Model (EARSM) with the experimental data measured by a Laser Doppler Velocimeter (LDV) was performed.

GRID CONVERGENCE INDEX (GCI)

The GCI was proposed by Roache (1994) and it represents a simple method for reporting grid-convergence studies without any restriction to integer refinement (e.g., grid doubling). The GCI is based on generalized theory of Richardson extrapolation involving comparison of solutions at different grid spacing. The GCI can be computed using two levels of grid; however, three levels are recommended in order to accurately estimate the order of convergence and to check that the solutions are within the asymptotic range of convergence. The authors have adopted the procedure for estimation of GCI proposed by Celik et al. (2008).

For three-dimensional (3D) calculations, a local grid size h_i was calculated using

$$h_i = \left[\frac{1}{N} \sum_{i=1}^{N} (\Delta V_i) \right]^{1/3} \tag{1}$$

where ΔV_i is the volume of the ith cell, and N is the total number of cells of the calculation domain. In this paper, the local cell size was used since the variables of interest were local, i.e. all local quantities depended on the position within the cross-section.

The simulations were run on three different sets of grids with a global constant refinement factor between the coarse and fine grids $\overline{r_{21}} = \overline{h_2}/\overline{h_1}$ and $\overline{r_{32}} = \overline{h_3}/\overline{h_2}$, where $\overline{h_1} < \overline{h_2} < \overline{h_3}$ and $\overline{h_1}$, $\overline{h_2}$ and $\overline{h_3}$ are the global grid sizes for fine, medium and coarse meshes accordingly. The local refinement factors $r_{21,i}$ and $r_{32,i}$ are dependent on the local cell size and therefore vary along the cross-section. The calculation of the local apparent order of accuracy p_i was performed using the expressions:

$$p_i = \frac{1}{\ln (r_{21,i})} |\ln|\varepsilon_{32,i}/\varepsilon_{21,i}| + q_i(p_i)| \tag{2a}$$

$$q_i(p_i) = \ln \left(\frac{r_{21,i}^{p_i} - s_i}{r_{32,i}^{p_i} - s_i} \right) \tag{2b}$$

$$s_i = 1 \cdot \text{sign} \left(\varepsilon_{32,i}/\varepsilon_{21,i} \right) \tag{2c}$$

where $\varepsilon_{32,i} = f_{3,i} - f_{2,i}$, $\varepsilon_{21,i} = f_{2,i} - f_{1,i}$, where $f_{1,i}$, $f_{2,i}$ and $f_{3,i}$ are the fine-, medium- and coarse-grid local solution of the variable of interest obtained with grid spacing $h_{1,i}$, $h_{2,i}$ and $h_{3,i}$, respectively. The local order of accuracy p_i is computed applying Newton–Raphson method to Equation (2a). This is an iterative procedure which does not work if either $\varepsilon_{32,i}$ or $\varepsilon_{21,i}$ is 'very close' to zero, i.e. when the difference between the local results obtained with the two adjacent meshes is almost negligible.

Local approximate relative error was calculated using:

$$e_{a,i}^{21} = \left| \frac{f_{1,i} - f_{2,i}}{f_{1,i}} \right| \text{ and } e_{a,i}^{32} = \left| \frac{f_{2,i} - f_{3,i}}{f_{2,i}} \right| \tag{3}$$

Roache (1997) defined the GCI for a particular grid as the error estimate multiplied by a factor of safety F_s:

$$\text{GCI}_i^{21} = \frac{F_s e_{a,i}^{21}}{r_{21,i}^{p_i} - 1} \tag{4}$$

$$\text{GCI}_i^{32} = \frac{F_s e_{a,i}^{32}}{r_{32,i}^{p_i} - 1} \tag{5}$$

where $F_s = 1.25$ has been adopted in this paper (Roache 1997).

NUMERICAL MODELLING

Calculation domain and boundary conditions

The domain, 0.785 m wide and 10 m long with a bottom slope 0.001, is exactly coincident with the experimental flume (Figure 1), and was discretized using three different meshes with hexahedral elements aligned to the main flow direction and refined close to the walls, free surface and transition zone between the main channel (MC) and the floodplain (FP). In Figure 1, H is the water level above channel bottom, h_b is the bankfull level above channel bottom, b is the MC bottom width, and B is the section width. For turbulence modelling purposes, the non-dimensional vertical coordinate, z^+, of the element closest to the bottom wall was kept around 30 for the FP and 50 for the MC, allowing the use of wall functions. The flow is biphasic (water + air) and therefore the free surface is within the calculation domain. A uniform velocity field with a water depth of 0.102 m and 5% turbulence intensity was prescribed at the inlet; while a hydrostatic pressure profile with zero velocity derivatives was set at the outlet. The upper boundary condition was prescribed on the air, at 0.05 m above the expected free surface, with free-slip wall to allow the free motion of the air along the channel, while facilitating the numerical robustness of the simulation. The bottom and side walls were prescribed with a non-slip boundary condition and an absolute roughness of 0.384 mm, obtained from the experiments.

Numerical scheme

The flow field was calculated using the commercial 3D CFD code ANSYS CFX 12.0. This code is based on the finite element-based control volume method, where the governing equations are discretized over each control volume. Advection
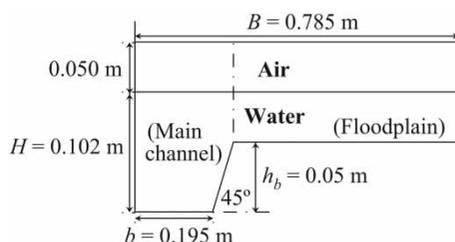
terms in Reynolds Averaged Navier-Stokes (RANS) equations are discretized using a second-order upwind scheme. Linear shape functions are used to evaluate spatial derivatives for all the diffusion terms and pressure gradient terms. The resulting system is then solved in a coupled manner, and the results are interpolated to the grid nodes. In this paper, the flow dynamics is modelled by numerically solving RANS equations for the water-air combination using the volume of fluid (VOF) method based on the idea of volume fraction (Hirt & Nichols 1981). There is a closure equation for the volume fraction, which states that both phases of volume fraction must add up to one at every computational cell. The free surface model is accompanied by an interphase sharpening algorithm, which guarantees a minimum diffusion of the volume fraction around the free surface. The stopping criterion for iterative calculations was set to be 10^{-5} for the normalized error in all equations, which led to an error of global mass flow imbalance smaller than 0.1%.

Turbulence closure model

The steady-state simulations were performed using the EARSM for the turbulence calculation in the RANS equations. The implementation is based on the EARSM of Wallin & Johansson (2000) in the form given by Hellsten (2004) for 3D flows. The EARSM represents an extension of the standard $k - \varepsilon$ model, and solves algebraic equations for six Reynolds stresses; the model is derived from the Reynolds stress transport differential equations and gives a nonlinear relation between the Reynolds stresses and the mean strain-rate and vorticity tensors (Wallin & Johansson 2000). The model solves the higher order anisotropic terms and thus, it is suitable to capture effects associated with secondary flows.

Method of analysis

Determination of the GCI in this paper, as described above, is based on the solution of large- and small-magnitude, yet very important, variables of interest. Particularly, all three water velocity components, turbulence kinetic energy (TKE), dissipation and Reynolds stresses, obtained with three different meshes were considered in the analysis. By calculating a GCI on three meshes and looking at the behaviour of GCI terms between two adjacent grids (i.e., between

Figure 1 │ Cross-section of the calculation domain of the compound channel.

meshes 1 and 2, and between meshes 2 and 3), one can make an assumption whether the solutions are within the convergence radius. Roache (1994, 1997) noted that it is neither necessary nor often desirable to use global grid refinement factor $\bar{r} = 2$ (the global refinement factor $\bar{r}$ was defined before in the GCI section), i.e. grid doubling (halving), instead he recommended a minimum 10% change in $\bar{r}$. In this paper, the authors adopted $\overline{r_{21}} = \overline{r_{32}} \approx 1.2$ in the cross-section direction of the flow for the water region where the turbulence terms are more sensitive to the grid resolution. The local refinement factors $r_{21,i}$ and $r_{32,i}$ range from 1 to 2.0 and from 1 to 3.4, respectively. In the streamwise direction of the flow, the mesh was not refined since it is the least sensitive flow direction, as expected for a developed flow; thus, the computational time of the simulation can be reduced without any direct effect on the credibility of the simulation (Hardy *et al.* 2003).

RESULTS AND DISCUSSION

Verification (GCI)

Since mesh doubling was not performed, for inter-mesh point-to-point comparison purposes, a cubic interpolation was performed between meshes 1 and 3 and meshes 2 and 3, corresponding to 1,843,200 elements in mesh 1, 1,337,600 elements in mesh 2, and 1,065,600 elements in mesh 3. For all three meshes, the number of elements in the x direction was kept equal to 200. The number of elements for the water region in the y and z directions for mesh 1, 2 and 3 are: 192×32, 152×28 and 148×20, respectively. In the air region, the number of mesh elements in the z direction was kept constant and equal to 16 elements. The GCI was determined for three components of velocity, TKE, dissipation and tangential Reynolds stresses only for the water region by considering a cross-section at 7.5 m from the inlet, where uniform flow was considered to be established. GCI values have been calculated for the 3,427 common data points (nodes) when meshes 1 and 2 were compared against mesh 3.

Figure 2 provides the results of the three velocity components obtained by meshes 1, 2 and 3, and presented only for the water region of the cross-section. The contours of u, v and w velocity components do not demonstrate significant evolution in response to grid resolution.

The averaged values over the cross-section, $\overline{\text{GCI}}$ and $\bar{p}$, are given in Table 1. As expected, the lowest absolute values of $\overline{\text{GCI}}$, 0.39 and 0.47%, are for the u velocity component, while the highest $\overline{\text{GCI}}$ values are for v and w velocity components, and Reynolds stresses $RSxy$ and $RSyz$. This is not surprising because these variables,
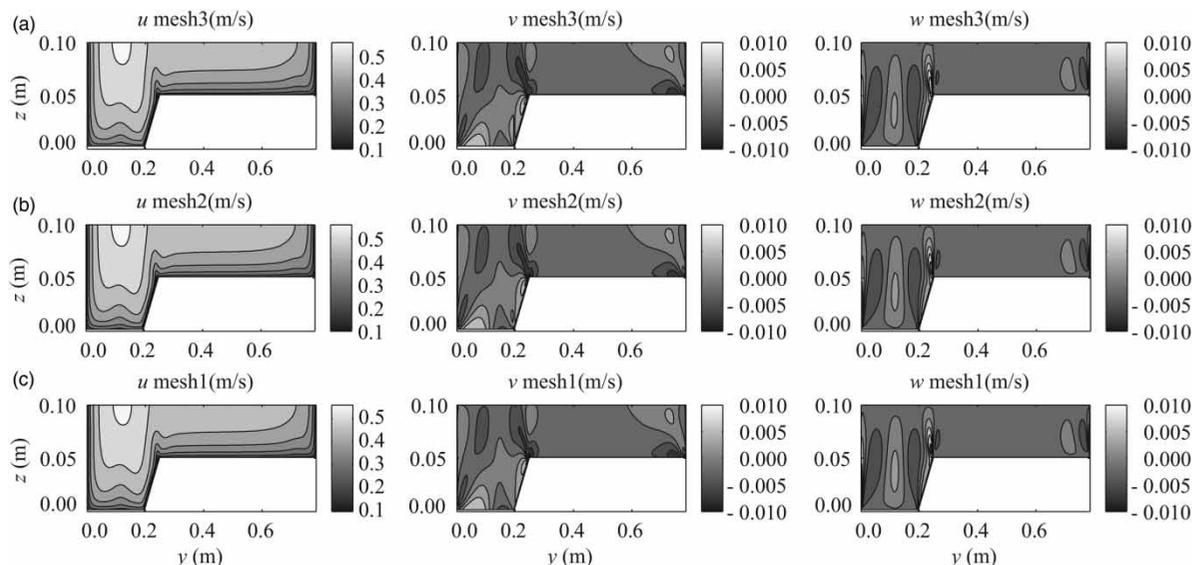

Figure 2 | Velocity components in the cross-section for water region: (a) mesh 3; (b) mesh 2; (c) mesh 1.

Table 1 │ Averaged $\overline{\text{GCI}}$ and $\bar{p}$ over the cross-section

Variable of interest	GCI32 (%)	GCI21(%)	$\bar{p}$ (−)
u component	0.47	0.39	6.3
v component	50.11	125.42	5.4
w component	806.45	220.21	5.6
TKE	6.42	5.68	4.2
Dissipation	−5.30	−6.27	3.5
Reynolds stress $RSxy$	76.65	41.67	5.9
Reynolds stress $RSxz$	9.99	8.95	3.2
Reynolds stress $RSyz$	195.43	77.83	5.9

representing secondary flow, have small magnitude and therefore are highly sensitive to grid resolution. Thus, high $\overline{\text{GCI}}$ values for v and w velocity components indicate that mesh resolution is not yet good for predicting secondary flow. But from Table 1 it is clear that, except for the v velocity component and dissipation, the $\overline{\text{GCI}}$ values decrease with the mesh refinement, thus $\overline{\text{GCI21}}$ shows better results than $\overline{\text{GCI32}}$. The averaged apparent order of accuracy $\bar{p}$ is always higher than the algorithm order (2nd order). It should be mentioned that for all variables there are negative values of local p_i near the wall, which means that asymptotic convergence is not achieved in that region.

The cross-section contours GCI21 and GCI32 for three velocity components, TKE, dissipation and tangential Reynolds stresses are presented in Figure 3. The scales in Figure 3 were limited to a maximum GCI value of 5% for each variable. The white spots on the plots represent the zones where the GCI is higher than 5%. For example, such zones of high GCI appear in the MC, near the interface region between MC and FP, where the secondary flows dominate, for v and w velocity components. For the u component, such zones of high GCI are much smaller and appear near the MC wall, where lower velocities are expected. For TKE and dissipation, these zones appear in both MC and FP and close to the walls, which means that is very likely that mesh resolution for these zones was not enough since it is well known that the largest dissipation rate occurs close to the walls (e.g., Fulgosi et al. 2003; Li et al. 2010). As for tangential Reynolds stresses, $RSxy$ and $RSyz$ present the worst results, for the former the white zones are mainly located in the region where the mixing (shear) layer develops, while for the latter those zones are present in both MC and FP,

where secondary flow is expected to be significant. Therefore, a higher spatial density of grid points is required to generate an adequate system definition of the shear layer and of secondary circulation, even though the streamwise flow is within a reasonable margin of error.

In order to reduce the $\overline{\text{GCI}}$ values, based on the GCI contours (Figure 3), meshes 1 and 2 were refined in transversal and vertical directions for the water region, mesh 3 was kept the same. The refinement was made in the horizontal direction near the lateral wall and in the mixing layer region, and in the vertical direction near the bottom and free-surface region. Afterwards, the global refinement factor became $\overline{r_{21}} = \overline{r_{32}} \approx 1.31$. The local refinement factors $r_{21,i}$ and $r_{32,i}$ range from 1 to 2.4 and from 1 to 3.7, respectively. The EARSM simulation was performed again on mesh 1 refined containing 2,436,000 hexahedron elements and on mesh 2 refined containing 1,564,000 hexahedron elements, corresponding to the number of elements in the y and z direction for the water region of 210×42 and 170×30, respectively. Then, these results together with the results of mesh 3 were used to calculate GCI21r (mesh 2 refined versus mesh 1 refined) and GCI32r (mesh 2 refined versus mesh 3), using the same methodology as mentioned above.

The new averaged values over the cross-section obtained with refined meshes, $\overline{\text{GCIr}}$ and $\overline{p_r}$, are shown in Table 2. The numerical results obtained with the refined meshes 2 and 1 did not show significant differences in general for all variables of interest. The refined $\overline{\text{GCI21r}}$ values (Table 2) are smaller than the non-refined $\overline{\text{GCI21}}$ values (Table 1) for some variables, as expected for u, v and w velocity components, but the opposite occurs for the other variables related to turbulence, which indicates that asymptotic convergence is still not attained. The averaged apparent order of accuracy $\overline{p_r}$ values (Table 2) are always smaller than the values obtained for non-refined meshes (Table 1), but closer to the algorithm order (2nd order).

All contours of GCI presented in Figure 4 show similar patterns; the white zones, that represent the areas where GCI is higher than 5%, are localized in the same positions as for the non-refined meshes (Figure 3), except for TKE and dissipation where those areas are pushed into the FP wall in the refined meshes. There are some nodes where the GCI is much higher than the average GCI of the cross-section, especially close to the wall where a special mesh
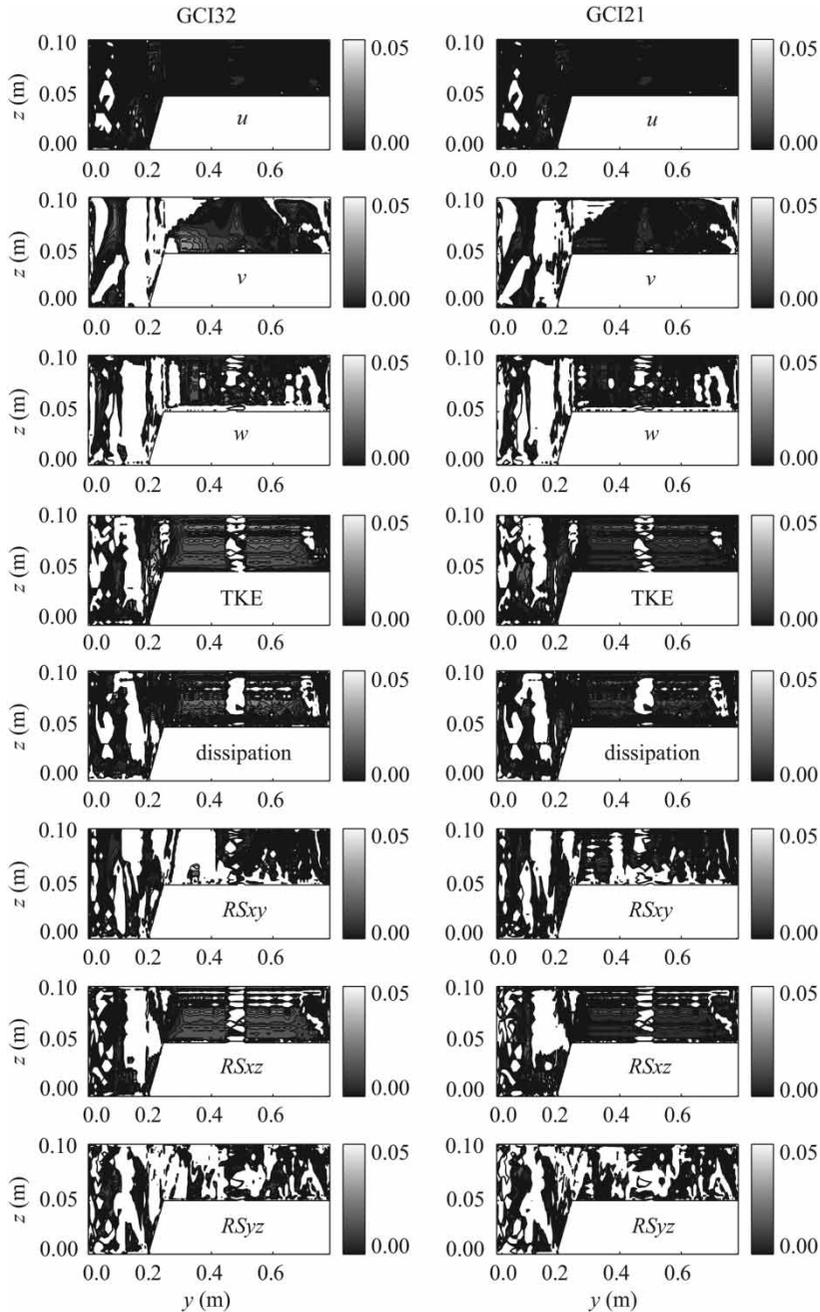
Figure 3 │ Contours of GCI for the three velocity components, TKE, dissipation and for the tangential Reynolds stresses at cross-section 7.5 m downstream from inlet.

resolution is required. When we compare the contours of Reynolds stress RSxy before (Figure 3) and after refinement (Figure 4), we can conclude that the area of white zones, where the GCI is higher than 5%, has decreased significantly according to the mesh refinement performed in the mixing (shear) layer region. However, the averaged $\overline{\text{GCI}}$ value for

Reynolds stress RSxy has increased in comparison to the non-refined mesh results (Tables 1 and 2, respectively), which is very likely due to the non-uniform spatial procedure of grid refinement and the high sensibility of this low magnitude variable to numerical inaccuracies. These inaccuracies are well explained by the lack of good resolution of the

Table 2 | Averaged $\overline{GCI}$ and $\overline{p_r}$ over the cross-section obtained with mesh 3, mesh 2 refined and mesh 1 refined

Variable of interest	$\overline{GCI32r}$ (%)	$\overline{GCI21r}$ (%)	$\overline{p_r}$ (−)
u component	0.50	0.23	1.8
v component	137.91	76.16	2.9
w component	50.77	165.93	2.2
TKE	18.72	17.74	1.8
Dissipation	32.83	31.62	1.4
Reynolds stress $RSxy$	592.59	106.42	2.9
Reynolds stress $RSxz$	46.90	44.30	1.6
Reynolds stress $RSyz$	97.09	89.60	2.2

viscous and buffer layers where important TKE, dissipation and Reynolds stresses are expected. Therefore, to reduce the GCI for the turbulence quantities, we need not only to refine the mesh, but also to provide an appropriate resolution of the close-to-wall turbulence, not obtained by $k - \varepsilon$ type wall functions as those used in this work. Nevertheless, further refinement of the mesh around the interface, where secondary flows are quite important, should improve results of GCI, especially for spanwise (v) and vertical (w) velocities, which are directly associated with these flows.

Analysing the last GCI results (Table 2) we can conclude that the numerical scheme is of an acceptable accuracy, especially for the u velocity component since the $\overline{GCI}$ is less than 1%. However, when the secondary variables are considered, like v and w components of velocity, and Reynolds stresses $RSxy$ and $RSyz$, the $\overline{GCI}$ values are dramatically high. Therefore, the typically very small v and w components, which are around 1–2% of the maximum streamwise velocity, are largely affected by interpolation and discretization errors implicit in calculation of the GCI (Equations (4) and (5)). Furthermore, there are few nodes within the flow section, where the values are much larger than 5%, mostly close to walls where large gradients are expected, affecting substantially the average cross-section $\overline{GCI}$. It is an issue as to which variable a scheme should be verified on. If the aim is to capture only the maximum longitudinal velocity, it can be assumed that the scheme has converged and the numerical accuracy is acceptable. However, if the aim is to capture all the processes of mass and momentum transfer between the MC and FP and secondary flows, the numerical accuracy of the scheme might

not be enough to predict lateral and vertical movement of the water. In such case, a further mesh refinement is necessary, or alternatively, the use of a higher order of the numerical scheme. Both alternatives lead to a more expensive computational cost.

Recalling the v and w results presented in Figure 2, they are quite similar for the three meshes and no visible improvement is seen, namely in what concerns intensity and location of secondary cells. This contradicts the GCI analysis that indicates a non-converged solution. Therefore, before trying a further mesh refinement the authors have decided to verify mesh quality using a different method. Thus, a linear regression analysis was performed between three data sets.

Linear regression analysis between meshes

In order to gain insight into discrepancies in the GCI values, the actual values of the different variables for mesh 3, and refined meshes 2 and 1 are considered. As with the GCI results, comparisons of refined meshes 1 and 2 are made to corresponding points on mesh 3, using a cubic interpolation. The results for u, v and w velocity components, TKE, dissipation and tangential Reynolds stresses are presented in Figure 5, where the solid line represents a linear regression line with zero intercept and dots represent the values of the variables in corresponding nodes between the two meshes. The comparison of variables in mesh 3 and refined mesh 2 (Figure 5) shows, taking into account correlation coefficients R close to unity, that velocities are overestimated by the coarser mesh, especially v and w; on the other hand turbulence quantities are underestimated, in particular dissipation and Reynolds stress $RSyz$. A clear improvement with mesh refinement can be seen by slopes closer to unity in refined meshes 2 and 1. The worst slope is obtained for dissipation, which is due to the fact that its values are higher near the boundaries and it is therefore a variable which is highly sensitive to grid resolution.

When the GCI values for the u velocity component are compared with the correlation coefficient and line slope, one can see that both methods give good results. Thus, we can conclude that mesh resolution is good enough and the results of streamwise velocity are mesh independent. However, when v and w velocity components and turbulence quantities are considered for refined meshes 1 and 2, there
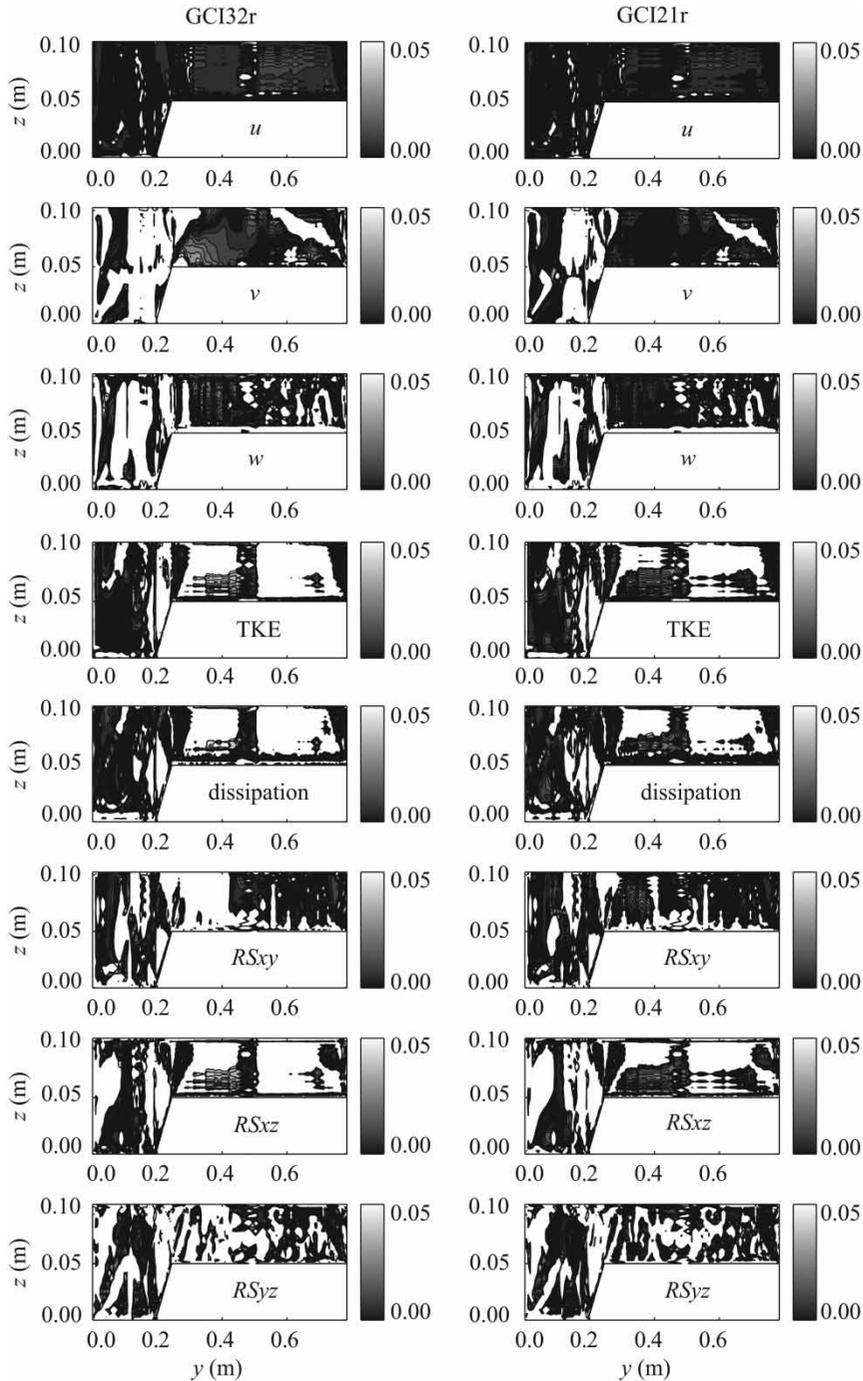
Figure 4 │ Contours of GCI for the three velocity components, TKE, dissipation and for the tangential Reynolds stresses at cross-section 7.5 m downstream from inlet obtained with refined meshes 1 and 2 and mesh 3.

is a fair agreement between the meshes with regression line slopes around 1 ± 0.08, in apparent contradiction with the GCI results. It means that for the compound channel case we cannot rely only on the GCI method in verifying the mesh quality. The GCI method is very sensitive when calculating low magnitude values, resulting in 'unrealistic' very large errors. However, both methods together are good for assessing the mesh quality.
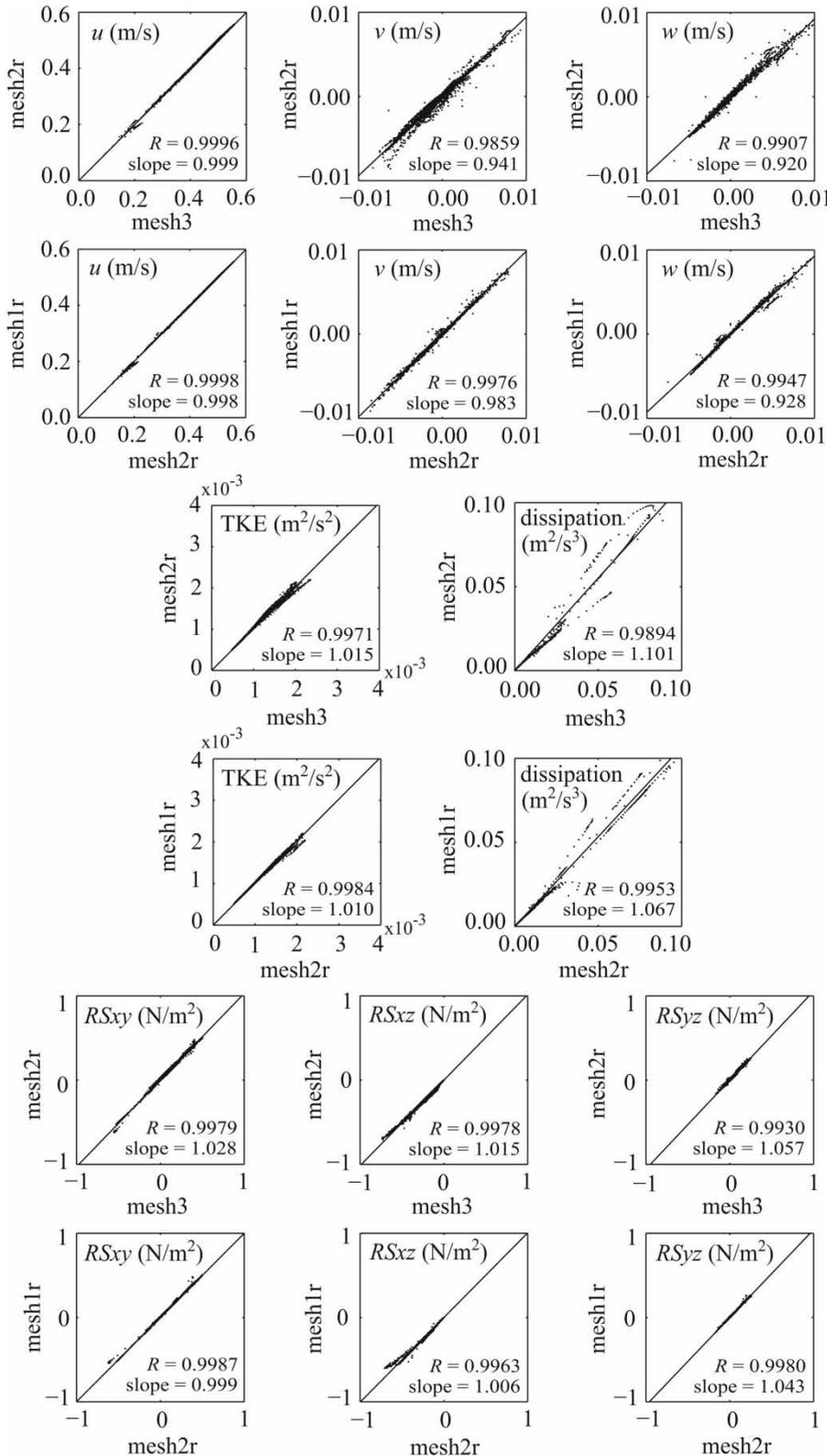
Figure 5 │ Linear regression analysis of *u*, *v* and *w* velocity components, TKE, dissipation and tangential Reynolds stresses for mesh 3 vs. mesh 2 refined and for mesh 2 refined vs. mesh 1 refined.

In summary, based on the results of linear regression analysis, as well as on GCI values, we can conclude that the use of both methods can overcome some drawbacks of GCI analysis and that mesh 2 refined is fine enough for 3D modelling, except for accurately predicting w, dissipation, Rxz and Ryz, especially near the walls.

Validation (experimental data)

In this part of the paper, the comparison of numerical and experimental results is performed. The experimental study was carried out in the Hydraulics Laboratory of the University of Beira Interior in a prismatic flume with a bed slope $S_0 = 0.001$, 10 m in length and with an asymmetric trapezoidal compound section (Figure 1). The uniform flow was established by imposing a discharge of 23.0 l/s which corresponds to a relative depth $h_r = (H–h_b)/H \approx 0.5$. The streamwise u and vertical w flow velocities were measured using a LDV. Positioning of the system was controlled by computer with 0.1 mm precision. The measurements were performed in back-scattering mode through the lateral glass-wall of the flume. The water depth was measured using a point gauge and acoustic probes; the total discharge was measured using an electromagnetic flow-meter installed in the recirculation pipe of the flume.

Numerical results are based on mesh 1 refined, described in previous sections. Figure 6 presents the numerical and experimental results for u and w velocity components for a cross-section 7.5 m downstream from the flume inlet. The experimental results presented here are only until lateral position $y = 0.4$ m, the maximum distance that LDV can measure in the experimental facility.

The numerical and experimental contours of the u velocity component show similar behaviour: the isovels bulge significantly upward near the upper interface as a result of secondary flow cells generated by wall turbulence anisotropy. The difference between numerical results and experimental data is essentially that the numerical model cannot capture the effect of free surface, where the maximum velocities occur below the free surface (Nezu 1994). This might be due to the missing modelling of free surface tension phenomenon in the computational model.

The numerical and experimental contours of the w component of velocity show a similar pattern: the positive and negative velocities are almost in the same locations, slightly shifted to the MC wall in the case of the experimental values. The presence of two secondary cells is observed, one rotating counter-clockwise located in the interface region and another rotating clockwise located in the MC, between the sidewall and the centre. The first secondary flow cell is responsible for pushing upwards particles with smaller velocities near the upper interface, causing the inflection of the isovels (Figures 6(a, b)). The intensity of this cell is slightly higher for the experimental results, which confirms the fact that Algebraic Stress Models underestimate the secondary flow (Bradshaw 1987). In the MC, near the lower interface, the interaction can be observed of the two secondary cells that direct the flow downwards and
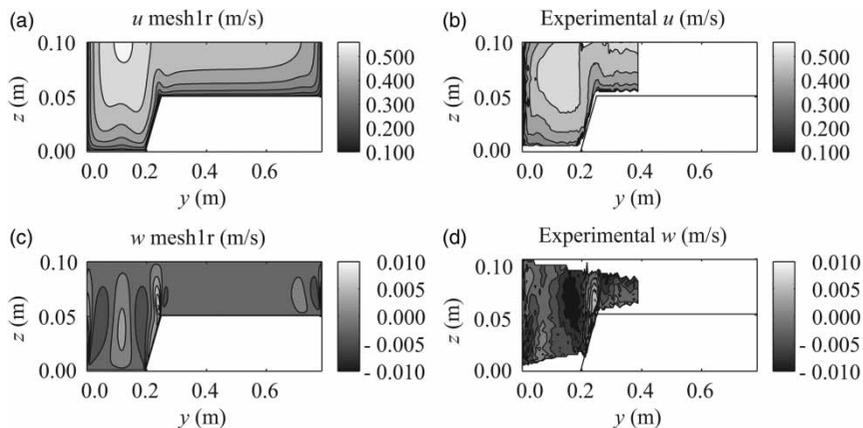

Figure 6 │ Comparison of u and w velocity components obtained numerically (a and c, respectively) and experimentally (b and d, respectively) at a cross-section 7.5 m downstream from inlet.
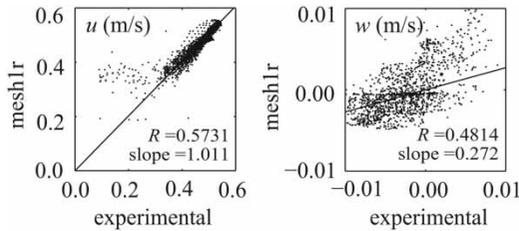
Figure 7 | Comparison between the velocity components *u* and *w* for mesh 1 refined and experimental data using linear regression analysis.

therefore inflect the isovels in that direction (Figure 6(a)). The numerical secondary flow cell in the MC (Figure 6(c)) shows the same effect, but the experimental one is significantly weaker and is not able to inflect the isovels downwards.

Linear regression analysis for *u* and *w* velocity components obtained experimentally and numerically is presented on Figure 7, for all points where experimental measurements were made. The comparison of the *u* velocity component, obtained numerically with mesh 1 refined and experimentally, suggests a good level of agreement. The major discrepancies are found for the lower velocities where the numerical model overestimates the experimental data, the low correlation coefficient also explains this, indicating that the model does not capture well what is happening near the walls. When a comparison is made for the *w* velocity component, a distinct area of disagreement exists. The dispersion of the results reflects the differences in experimental and numerical locations of the secondary cells. It is observed that generally the numerical model underestimates the experimental *w* velocity component.

The cross-section average relative error between numerical and experimental results for the *u* velocity component is 1.15%, and 329.52% for the *w* velocity component. The relative error for vertical velocity *w* is too high; this is due to very small values of the *w* velocity component and the previously mentioned error in secondary flow. The value of vertical velocity *w* is two orders of magnitude smaller than the value of longitudinal velocity *u* and any, even very small, difference in the value between numerical results and experimental data results in a large relative error. Also there is an influence of the cubic interpolation of numerical results into the coarse experimental mesh.

CONCLUSION

In this paper, the GCI method was adopted for the verification of 3D CFD simulations of compound channel flow. The GCI is a recognized technique which follows a standard editorial policy statement for the control of numerical accuracy.

The verification has shown that when meshes 1, 2 and 3 are considered for calculations, the GCI has the smallest values for downstream component of velocity (*u*) and the highest for higher order parameters. After the refinement of the mesh, although some improvements in $\overline{GCI}$ can be observed, the higher order variables still present an oscillating $\overline{GCI}$ behaviour, either increasing from coarse to finer meshes or from non-refined to refined meshes. It must be noted that the high $\overline{GCI}$ values are mostly due to a few number of cells located near the walls, where clearly one cannot assume that asymptotic convergence is achieved.

In addition to the GCI method, the authors have adopted a linear regression analysis to verify the mesh quality. This analysis has shown a much better level of agreement between the meshes with regression line slopes close to unity for most variables, and converging to unity with mesh refinement. Nevertheless, velocity components *v* and *w* are overestimated and turbulent quantities are underestimated by coarser meshes (mesh 3 and mesh 2 refined), in particular dissipation and Reynolds stress *RSyz*. The dissipation rate is known to be one of the most difficult turbulence parameters to model and the Reynolds stress *RSyz* is linked to bottom turbulence. The Reynolds stress *RSxy* presents very good results for the finer mesh, indicating that the refinement in the mixing layer region was more effective than near the walls. Merging GCI and linear regression analysis, we can conclude that the refined mesh has satisfactorily converged for most variables.

The validation has shown a fair agreement between numerical and experimental results. For the streamwise velocity (*u*), the model is capable of simulating the entire flow field, except the near-wall region. For the vertical velocity (*w*), the results show that the model is able to simulate secondary flow, although the location and intensity of secondary cells differs from the experimental ones. This is a known characteristic of Algebraic Stress Models, and

therefore should not be totally attributed to mesh dependence.

Summarizing, it can be stated that the methods for solution verification used in this paper, GCI method and linear regression analysis, are good for assessing the credibility of the simulations. From the discussion above, it is clear that, although the GCI method is mathematically well-founded, when small value variables are considered the method should be complemented with other methods, such as linear regression analysis.

ACKNOWLEDGEMENTS

REFERENCES

Bradshaw, P. 1987 Turbulent secondary flows. *Ann. Rev. Fluid Mech.* **19**, 53–74.

Celik, I., Chen, C. J., Roache, P. J. & Scheurer, G. 1993 Quantification of uncertainty in computational fluid dynamics. ASME Fluids Engineering Division Summer Meeting, ASME Publ. No. FED-Vol. 158, Washington, DC, Jun. 20–24.

Celik, I., Ghia, U., Roache, P. J., Freitas, C. J., Coleman, H. & Raad, P. E. 2008 Procedure for estimation and reporting of uncertainty due to discretization in CFD applications. *J. Fluids Eng.* **130**, 078001-1–078001-4.

Celik, I., Hassan, Y., Hughes, D., Johnson, R. & Sommerfeld, M. 1994 *Experimental and Computational Aspects of Validation of Multiphase flow CFD Codes*. The American Society of Mechanical Engineers United Engineering Center, FED-Vol. 180, New York.

Coleman, H. W. & Stern, F. 1997 Uncertainties and CFD code validation. *J. Fluids Eng.* **119**, 795–803.

Freitas, C. J. 1993 Journal of fluids engineering editorial policy statement on the control of numerical accuracy. *ASME J. Fluids Eng.* **115**, 339–340.

Fulgosi, M., Lakehal, D., Banerjee, S. & De Angelis, V. 2003 Direct numerical simulation of turbulence in a sheared air-water flow with a deformable interface. *J. Fluid Mech.* **482**, 319–345.

Hardy, R. J., Lane, S. N., Ferguson, R. I. & Parsons, D. R. 2003 Assessing the credibility of a series of computational fluid dynamic simulations of open channel flow. *Hydrol. Processes* **17**, 1539–1560.

Hellsten, A. 2004 New Two-Equation Turbulence Model for Aerodynamics Applications. Laboratory of Aerodynamics, Report No. A-21, Helsinki University of Technology, Series A, 2004, ISBN 951-22-6933-3. Doctoral dissertation.

Hirt, C. W. & Nichols, B. D. 1981 Volume of fluid (VOF) method for the dynamics of free boundaries. *J. Comput. Phys.* **39** (1), 201–225.

Li, X.-X., Liu, C.-H. & Leung, D. Y. C. 2010 Parallel FEM LES with one-equation subgrid-scale model for incompressible flows. *Int. J. Comput. Fluid Dyn.* **24**, 37–49.

Morvan, H. P. 2005 Channel shape and turbulence issues in flood flow hydraulics. *J. Hydraul. Eng.* **131**, 862–865.

Morvan, H. P., Pender, G., Wright, N. G. & Ervine, D. A. 2002 Three-dimensional hydrodynamics of meandering compound channels. *J. Hydraul. Eng.* **128** (7), 674–682.

Nezu, I. 1994 Compound open-channel turbulence and its role in river environment – Significance of secondary currents. 9th Congress of APD-IAHR, Keynote Address, Singapore.

Oberkampf, W. L. 1994 A proposed framework for computational fluid dynamics code calibration/validation. *AIAA Paper No. 94-2540, 18th AIAA Aerospace Ground Testing Conference*, Colorado Springs, CO.

Oberkampf, W. L. & Trucano, T. G. 2002 Verification and Validation in Computational Fluid Dynamics. Sandia Report SAND2002-0529. Sandia National Laboratories, Albuquerque, NM.

Roache, P. J. 1994 Perspective: a method for uniform reporting of grid refinement studies. *J. Fluids Eng.* **116**, 405–413.

Roache, P. J. 1997 Quantification of uncertainty in computational fluid dynamics. *Ann. Rev. Fluid Mech.* **29**, 123–160.

Roache, P. J. 1998a *Verification and Validation in Computational Science and Engineering*. Hermosa Publishers, Albuquerque, NM.

Roache, P. J. 1998b Verification of codes and calculations. *AIAA J.* **36** (5), 696–702.

Roache, P. J., Ghia, K. N. & White, F. M. 1986 Editorial policy statement on control of numerical accuracy. *ASME J. Fluids Eng.* **108**, 2.

Sterling, M., Beaman, F., Morvan, H. & Wright, N. 2008 Bed-shear stress characteristics of a simple, prismatic, rectangular channel. *J. Eng. Mech.* **134** (12), 1085–1094.

Wallin, S. & Johansson, A. V. 2000 An explicit algebraic Reynolds stress model for incompressible and compressible turbulent flows. *J. Fluid Mech.* **403**, 89–132.